

CLASSIFICATION OF 3D TESSELLATIONS

I. SAXL, P. PONÍŽIL

ABSTRACT. Classification of Voronoi tessellations generated by various point processes is proposed and discussed.

Абстракт. Классификация областей Дирихле (Вороного) генерированных различными точечными процессами предложена и и обсуждена.

1. INTRODUCTION

The broad collection of space-filling cell systems – tessellations – that are simultaneously covering and packing is encountered by examining grains of polycrystals. Beside highly uniform systems with regular grains of similar size and shape, also extremely locally inhomogeneous systems occur in practice as results of exaggerated grain growth during certain thermal treatment of materials, in particular of steels. They consist of huge isolated or contiguous cells separated by regions of very small cells. Suitable stochastic models of such space-filling systems are convex polyhedral Voronoi tessellations generated by various random or deterministic point processes [6]; they are called the *tilings* if the cells are translation equivalent. Frequently encountered generating processes and shape properties of the corresponding tessellations are reviewed in [13].

Simultaneously with a given spatial tessellation T , also the tessellations T' , T'' induced by it in the whole system of section planes and lines are considered. In practice, only the partial information contained in such sections is directly accessible (crystals are usually opaque) and the data gathered by their examination serves as the basis of any inference concerning the properties of the original spatial tessellation.

The elementary characteristics of tessellations are their *intensities*: the mean numbers of cells λ , profiles λ' and chords (intercepts) λ'' per unit volume (area, length) of the embedding spaces. The detailed description of a tessellation is given by the distributions of its cell characteristics. Size characteristics are cell volume v , surface area s , mean breadth w (also the mean calliper or Feret diameter), perimeter p (the total edge length), induced cell (profile) area v' , its perimeter s' and chord (intercept) length v'' . All size characteristics are homogeneous functions (of different degree) of the intensities λ^\bullet , which are scale quantities only from the view point of cell shape and arrangement. Clearly, $\mathbf{E}v = 1/\lambda$, $\mathbf{E}v' = 1/\lambda'$, $\mathbf{E}v'' = 1/\lambda''$. The important global characteristics of T are the areal intensity $S_V = \lambda \mathbf{E}s/2$ (the mean total cell boundary area per unit volume) and the length intensity $L_V = \lambda \mathbf{E}p/3$ (the mean total edge length per unit volume). The analogical length intensity of T' is $L_A = \lambda' \mathbf{E}s'/2$ (the mean total length of profile boundaries per unit area).

2000 *Mathematics Subject Classification*. 60-04, 60D05, 60G55.

Key words and phrases. Voronoi tessellations, cell size characteristics, $w - s$ diagram.

The research was supported by Grant No. 304/00/1622 of GA ČR (I.S.), by the Ministry of Education of the Czech Republic (contract No. 281100015 - P.P.) and by Grant MSM 113200008.

2. PREVIOUS ATTEMPTS

Before describing the proposed classification scheme, the earlier attempts to categorize tessellations will be described. Herman, Wendrock & Stoyan [3] proposed to classify planar tessellations by their coordinates $\{p, q\}$ in the space of parameters of selected two parametric unimodal distributions $f(x; p, q)$ of the cell area a . The choice of lognormal, Maxwell and γ distributions was examined for several tessellations generated by hard-core (variable packing density) and cluster (variable cluster size and mean cardinality) point processes. However, the choice of the distribution is rather arbitrary and its parameters are only loosely connected with the geometric characteristics of the examined tessellations. Further, it is clearly sufficient to classify only the unit tessellations. Then certain fixed relation, $p = p(q)$, between the distribution parameters must hold and, consequently, all tessellations lie on the curve $\{q, p(q)\}$. The standard γ -distribution with zero threshold, $f(x) = p^q x^{q-1} \exp(-px) / \Gamma(q)$, has the moments $\mu'_1 = q/p$, $\mu'_2 = q/p^2$. Hence, all unit tessellations lie on the ray $p = q$, $q \geq 0$ and $q = 1/\text{var } a$, the point $p = q = 1/0.28$ describes the 2D Poisson-Voronoi tessellation. Tessellations generated by clustered point patterns lie in the interval $p \in (0, 1/0.28)$ and those ones generated by hard- and pseudo-hard-core patterns cover the interval $p \in (1/0.28, \infty)$; all tilings are gathered in the point at infinity independently of their cell shape.

A similar attempt [7] (tessellations generated by Boolean cluster fields) was based on the generalized γ -distribution proposed for the Poisson-Voronoi tessellation (PVT) by Hinde and Miles [4]. Standard difficulties in the estimation of the γ -distribution parameters produced a considerable scatter of results and their interpretation was difficult. Moreover, in tessellations generated by point cluster processes with high cluster cardinality and small cluster size, the distributions of all size characteristics are multimodal [8], [9].

Lorz [5] proposed a non-parametric approach based on the coefficient of variation of the cell area $CV a$ and on the mutual dependence between the quantiles $q_\alpha(a)$ vs $q_{1-\alpha}(a)$ for planar sections of 3D tessellations. As in the previous case, the direct interpretation of the obtained maps is rather obscure and the basic geometric characteristics of tessellations remain in the background. However, the importance of the coefficients of variation of the cell content has been properly recognized in Lorz' approach.

In order to stress the importance of the cell properties in the classification scheme, Saxl and Ponížil [11] constructed maps with rectangular coordinates $\{\mathbf{E}X, CV v\}$, where X were selected characteristics like s, w , cell shape properties *etc.* In such maps, every tessellation was characterized by a point and tessellations of considered types lie on the parametric curves $\{\mathbf{E}X(t), CV v(t)\}$ with t being a selected parameter of the generating point process – see Fig. 4 in [1] showing such a map for 3D tessellations generated by hard-core and pseudo-hard-core point. Unfortunately, the numerous maps (for T as well as for T') were neither illustrative nor helpful in the size and shape estimation.

An extensive need of versatile classification emerged in the connection with the stereology of line and planar sections of simulated 3D tessellations. In the framework of the long-term project, the database has been created of geometric cell properties covering few hundreds of different systems. The fundamental requirement was to include beside the original 3D tessellations also the corresponding 2D and 1D induced descendants. Under such a condition, the solution was straightforward.

3. STEREOLOGY OF TESSELLATIONS

The basic stereological formula relating intensities of the induced and the original tessellations is [16]

$$(1) \quad \lambda = \lambda' / \mathbf{E} w = \lambda'' / \mathbf{E}(s/4).$$

It can be formally rewritten as follows (for an extensive set of similar formulae see [2]):

$$(2) \quad \lambda = c'(T)\lambda^{3/2} = c''(T)\lambda'^3, \lambda' = c(T)\lambda''^2,$$

where the scale independent factors related to cell shape and size distributions are

$$(3) \quad c'(T) = \lambda^{-1/2}(\mathbf{E}w)^{-3/2}, c''(T) = \lambda^{-2}\mathbf{E}(s/4)^{-3}, c(T) = (c''(T)/c'(T))^{2/3}.$$

For unit tessellations, they simplify to power functions of the mean characteristics:

$$(4) \quad c'(T) = (\mathbf{E}w)^{-3/2}, c''(T) = (\mathbf{E}s/4)^{-3}, c(T) = \mathbf{E}w/(\mathbf{E}s/4)^2.$$

If the tessellation is *normal* (four cells meet in a vertex, three cells meet along an edge and two neighbouring cells have a common boundary facet) then $p = 12w$ and $c(T) = L_V/S_V^2$.

Summarizing these results, $\mathbf{E}w$ determines the intensity λ' and equals $L_V/4$ in the case of a unit normal tessellation. Similarly, $\mathbf{E}s$ governs the intensity λ'' and equals $S_V/2$ of unit tessellations. Hence $\mathbf{E}w$, $\mathbf{E}s$ are the basic characteristics describing the global intensities S_V , L_V (in general, $p \propto w$ for any convex cell by Hadwiger characterization theorem [16]) and, moreover, relating simply the intensities of the original and induced tessellations. Then it is quite natural to base the classification on them. On the other hand, neither λ nor $\mathbf{E}w$, $\mathbf{E}s$ can be inferred from the induced tessellations without some additional assumptions.

4. $w - s$ DIAGRAM AND ITS CONSTRUCTION

In the $w - s$ diagram [14], any unit (i.e. $\mathbf{E}v = 1$ tessellation is characterized by its mean cell characteristics $\mathbf{E}w$, $\mathbf{E}s$ in the $\{w, s\}$ plane. Tessellations generated by point fields $\Phi(t, u, \dots)$ of the same type with parameters t, u, \dots are then represented by parametric curves $\{\mathbf{E}w_{u, \dots}(t), \mathbf{E}s_{u, \dots}(t)\}$, where t is the chosen variable parameter (e.g. the mean cluster cardinality N) and the remaining parameters (e.g. the cluster size) are fixed. Other characteristics of the examined tessellations (shape factors, quantiles, and, in particular, coefficients of variation of cell contents $\text{CV } v$, $\text{CV } v'$, $\text{CV } v''$, are evaluated simultaneously and can be plotted as labels in selected curve points. Certain correlation between the tessellation position and its statistical properties, (coefficients of variation of cell volume, profile area and chord length etc.) is clearly apparent – see below. In view of the stereological relations between the intensities of the original and induced tessellations, the diagram can also be considered as the $\lambda' \text{ vs } 4\lambda''$ diagram of unit 3D tessellations. The mean probability that a cell is sampled by a section plane (line) is proportional to $\mathbf{E}w(\mathbf{E}s/4)$, respectively. Consequently, the smaller are $\mathbf{E}w$, $\mathbf{E}s$, the smaller number of cells is hit by the section plane, the smaller are the intensities of the induced tessellations and the higher must be the factors c', c'' . Thus the $w - s$ diagram can be considered as a basic tool for understanding the stereological problems encountered in estimating the properties of spatial tessellations from their induced tessellations.

The $w - s$ diagram is constructed gradually in what follows. For the definitions of various generating point processes and the basic tessellation properties see [16], [17].

4.1. Tilings, random hard-core and pseudo-hard-core tessellations. Two types of tilings have been considered:

a) *tilings generated by cubic lattices*, namely by the simple, body-centred and face centred lattices (the prototiles are cube, regular tetrakaidecahedron and rhombic dodecahedron, respectively). Their positions (denoted by diamond symbols) in the $w - s$ diagram are shown in Fig. 1.

b) *monoclinic lattices* with the angle $\alpha = \pi/3$ and lattice constants $\{v, v, c = qv\}$ with the variable axes ratio q (the prototiles are regular hexagonal prisms – long rods at high values of q and thin plates in the opposite case).

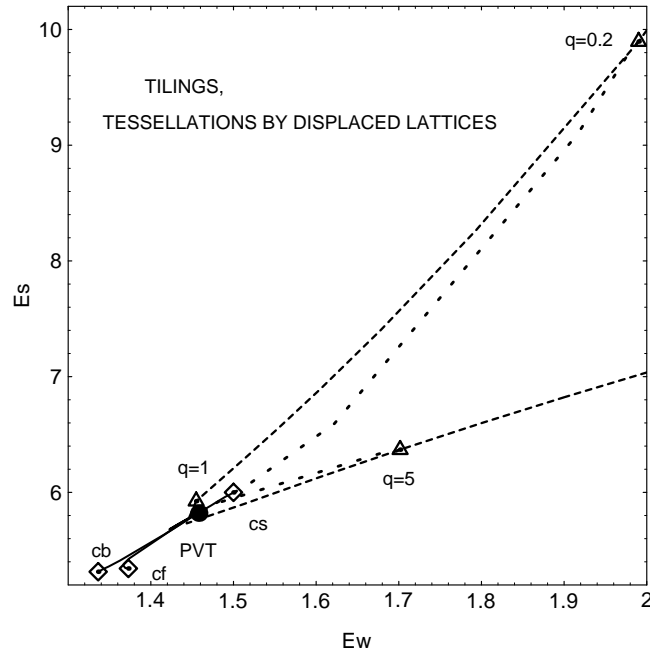


Fig. 1 Central and right upper part of the $w - s$ diagram: tilings and tessellations generated by displaced lattices (see the text).

| | s | w | f | g | p/w | CV v' |
|---------------------------|-------|-------|---------|--------|-------|---------|
| tetrakaidecahedron (cb) | 5.315 | 1.336 | 0.800 | 0.868 | 12 | 0.532 |
| rhombic dodecahedron (cf) | 5.345 | 1.375 | 0.735 | 0.860 | 12 | 0.565 |
| cube (cs) | 6 | 1.5 | 0.566 | 0.724 | 12 | 0.642 |
| hexagon. prism $q = 0.01$ | 5.08 | 59.9 | 0.0146 | 0.0229 | 8.01 | |
| 0.1 | 2.43 | 14.2 | 0.133 | 0.198 | 8.13 | |
| 1.51 | 1.430 | 5.73 | 0.653 | 0.775 | 9.34 | |
| $\sqrt{3}$ | 1.433 | 5.72 | 0.649 | 0.778 | 9.47 | |
| 10. | 2.19 | 7.43 | 0.181 | 0.525 | 11.1 | |
| 100. | 8.07 | 14.9 | 0.00363 | 0.186 | 11.9 | |

Tab. 1 Selected properties of considered unit ($v = 1$) tilings.

Important properties of such tilings are summarized in Tab. 1. Note the variable p/w ratio in hexagonal tilings: horizontal four-valent edges prevail at low values of q and the fibre process of tile edges has a pronounced planar anisotropy whereas three-valent vertical edges are dominant at high values of q (linear anisotropy of edges). In the $w - s$ diagram – Fig. 1, hexagonal prismatic tilings are represented by the v-shaped curve, plates with $q = 1, 0.2$ in its upper part and rods $q = 5$ in its lower part are denoted by triangles.

w and s of isohedral tiles have lower bounds $((6/\pi)^{1/3}$ and $(36\pi)^{1/3}$) by the isoperimetric and Bierbach inequalities, resp., but no upper bounds and the right upper part of the $w - s$ diagram is filled by tilings with flattened or elongated cells. Isohedral tiling by unit hexagonal prisms with the height to edge ratio q can serve as an example: $s = 2.7495(1 + 1.1547q)/q^{2/3}$ and $w = 0.3637(3 + q)/q^{1/3}$. The minimum values of w, s are attained near the tip of the v-shaped curve $\{w(q), s(q)\}$ at $q = \sqrt{3}$ and $q = 1.5$, resp., and $w, s \rightarrow \infty$ for $q \rightarrow 0$ (hexagonal plates) as well as for $q \rightarrow \infty$ (hexagonal rods). Hence $c', c'' \rightarrow 0$ in the both limit cases, whereas $c \rightarrow 0$ only at $q \rightarrow 0$ and $c \rightarrow 0.577$ for $q \rightarrow \infty$ (lower branch).

Curves $\{\mathbf{E}w(a), \mathbf{E}s(a)\}$, $a \in [0.005, 10]$, joining the tiling points cb, cf and cs with the PVT point (denoted by the black circle in Fig. 1) describe the tessellations generated by the corresponding Bookstein models [10] on the cubic lattices (called also the displaced lattice processes because each lattice point is independently shifted by a random vector ξ having a normal 3D distribution $N(0, \Xi)$ with $\Xi = a^2 \mathcal{I}$, where \mathcal{I} is a unit matrix) with the increasing standard deviation a . Note the slight overshooting of the curves in the neighbourhood of the PVT point. Similarly, the dashed curves joining the $q = 0.2$ and $q = 5$ points with the PVT point are generated by the monoclinic displaced lattices (the range of a as above).

Tessellations generated by the full range of Matérn type I (MI, hard-core diameter $0 \leq \delta \leq 0.34$, maximum attained volume fraction of random sphere packing $f_{\max} = 0.04$) and type II (MII, $0 \leq \delta \leq 0.62$, $f_{\max} = 0.125$) processes and by the simple sequential inhibition process (SSI, $0 \leq \delta \leq 0.9$, $f_{\max} = 0.38$) [10] are shown in Fig. 2a – the curves $\{\mathbf{E}w(\delta), \mathbf{E}s(\delta)\}$. In spite of different definitions of the processes, the positions of the tessellations generated by them and by the body-centred displaced lattices nearly coincide.

Finally, the positions of the tessellations generated by the conditional Strauss process [1] are presented in Fig. 2b. The generating processes at three choices of the variable radius $R = 0.72, 0.865$ and 1.44 are examined at different values of the interaction parameter γ – the curves $\{\mathbf{E}w(\gamma)_R, \mathbf{E}s(\gamma)_R\}$, $\gamma \in [0.01, 1]$ (the value of $\gamma = 1$ corresponds to the Poisson point process, hence to the Poisson-Voronoi tessellation). Note that again when R is close to the theoretical value of the hard-core parameter for the densest spherical packing, then the positions of the tessellations at decreasing γ closely follow the positions of the tessellations generated by displaced body-centred lattices, and in this range also by the face-centred displaced lattices. On the other hand, when R is considerably greater than the theoretical value, they approach the region of flat and rod-like cells (higher values of $\mathbf{E}w, \mathbf{E}s$).

4.2. Tessellation generated by point cluster fields. Two types of point cluster fields have been considered: Bernoulli cluster fields as a generalization of the Neyman-Scott process have been introduced in [15] and shortly described in [14]. The broad range of cluster cardinality has been examined: $N \in [1, 999]$ for Poisson globular (PG) clusters and $N \in [1, 200]$ for Poisson spherical (PS) clusters. The cluster diameter was $\delta = 0.01$ in the units of the mean nearest neighbour distance of

the parent Poisson point process, hence the clusters were small and only very rarely overlapping. The $w - s$ diagram of the tessellations generated by the Neyman-Scott cluster field (the probability of cluster implantation into a parent point $p = 1$) is shown in Fig. 3 – note the extreme range of the values of $\mathbf{E}w$, $\mathbf{E}s$ attained. The PG tessellations are strictly bimodal whenever N exceeds 4; the position of the lower value mode (corresponding to small *inner cells* [8], [9], [13]) of the cell volume distribution is nearly independent of N . PS tessellations are unimodal with wedge-, rod- and plate-like cells. The difference between the the positions of the tilings by hexagonal rods and PS tessellation is rather small (see the right upper corner of Fig. 5 and compare Fig's 1 and 3).

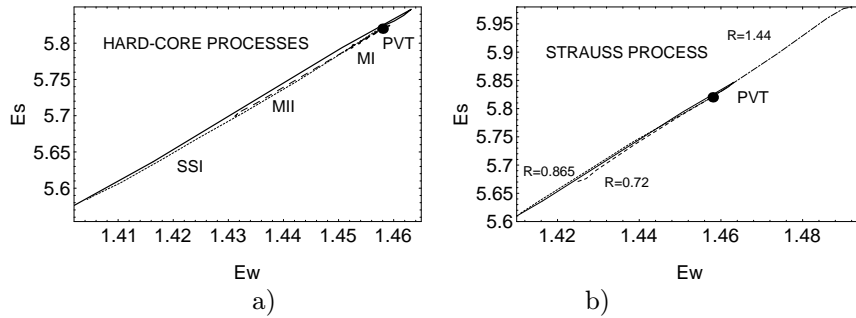


Fig. 2 Central part of the $w - s$ diagram with hard-core (a) and Strauss (b) processes; tessellations generated by the body-centred displaced lattices are shown for the comparison (full lines).

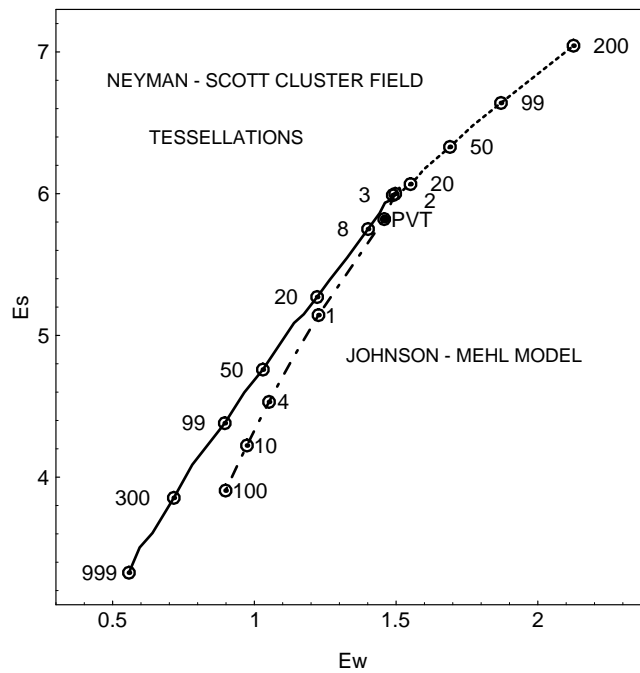


Fig. 3 $w - s$ diagram of tessellations generated by the Neyman-Scott cluster fields with globular (full line) and spherical (dotted line) clusters of the mean cardinality N shown as a label in selected points. Johnson-Mehl model with the variable parameter $0 \leq \beta \leq \infty$ shown as a label in several points.

For comparison, the position of the well-known Johnson-Mehl model [16] is shown. The Poisson-Voronoi tessellation can be obtained by the simultaneous isotropic constant rate growth of grains from point germs; the growth locally stops whenever two nuclei meet, the process of germs is the stationary Poisson point process. The same type of growth is assumed in the Johnson-Mehl model. However, the germs are nucleated continually at the rate $I = \alpha t^{\beta-1}$, starting at the time $t = 0$, $\beta \geq 0$ is the model parameter; the Poisson-Voronoi tessellation corresponds to its lower bound. The rejection rule is applied, namely the germs nucleated within an already growing grain are not accepted. The cells are mildly non-convex, their size dispersion increases with the growing parameter β : $\text{var } v \rightarrow \infty$ for $\beta \rightarrow \infty$. The whole range $0 \leq \beta \leq \infty$ of the JM model is shown in Fig. 3.

The last examined component of the $w - s$ diagram are tessellations generated by the Bernoulli cluster fields with the implantation probability $0 \leq p \leq 1$. Their construction and the approximate calculation of their properties for small values of the cluster diameter δ are described at length in [15]. For globular clusters, the distributions of the cell volumes are trimodal (small inner and greater outer cells generated by cluster points and huge cells of the cluster free points of the original parent process points). As the mean value of the cluster cardinality N need not be an integer in general, positions of such tessellations cover the whole area of the $w - s$ diagram lying below the curve describing the tessellations generated by the Neyman-Scott fields of spherical and globular clusters. Selected theoretically calculated curves $\{\mathbf{E}w(p)_N, \mathbf{E}s(p)_N\}$, $p \in (0, 1)$ are shown in Fig. 4. The effect of increasing values of δ on such curves, namely the gradual shrinkage of loops, is described in [14], [15].

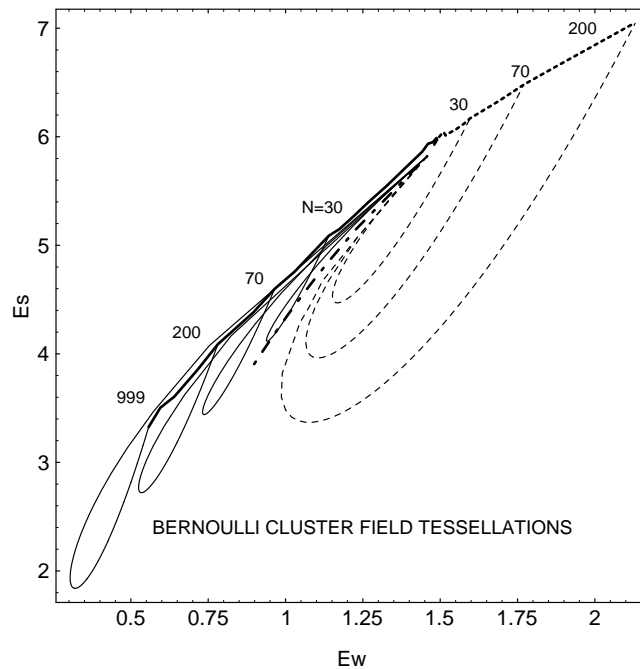


Fig. 4 $w - s$ diagram of tessellations generated by the Bernoulli globular (self-intersecting loops) and spherical (dashed incomplete loops) cluster fields; $\delta = 0.01$. The curves introduced in Fig. 3 are plotted for the comparison.

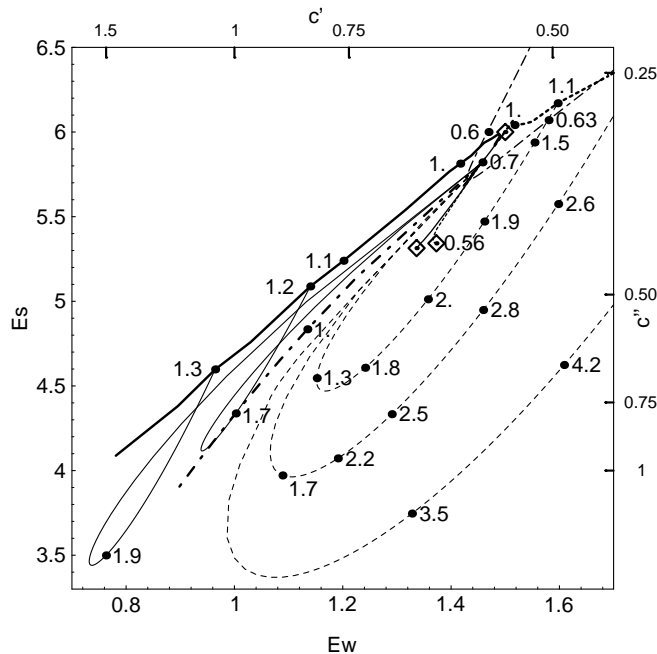


Fig. 5 The central part of the $w - s$ diagram labelled by the values of the coefficient of variation $CV v'$.

The characteristics of simulated tessellations can be found and the $w - s$ diagrams with various labels (tessellation parameters, coefficients of variation) interactively constructed and downloaded at the Internet page

<http://fyzika.ft.utb.cz/voronoi/>

– see an example in Fig. 5.

4.3. General features of the $w - s$ diagram. Tessellations formed by cells the widths $w(u)$ (recall that the width $w_C(u)$ of a convex body C is the distance of the parallel support planes with the normal u) of which are only mildly dependent on the orientation u of their support planes are called *equiaxial*; the common examples are tessellations generated by displaced cubic lattices and PVT. Equiaxial tessellations with a moderate unimodal size dispersion of cell volumes are cumulated in the neighbourhood of the PVT point $\{1.458, 5.821\}$ and are suitable models of the cell arrangement in living tissues as well as of grains in polycrystals of many face-centred metals and alloys [19].

Figure 5 demonstrates that in this area of the $w - s$ diagram, the lowest values of the coefficients of variation of cell contents (volumes, areas lengths) are attained. $CV v$ has only one component describing the size distribution of cell volume; its value is zero for all tilings. In the induced tessellations, also the variability of sectioning contributes to the values of $CV v'$ and $CV v''$ whereas the original cell volume dispersion is considerably obscured by the weighted profile sampling (planes sample the cells by their widths, lines by their projection areas), the result of which is a preferred sectioning of greater cells.

Tessellations with plate- or rod- or wedge-like cells and their mixtures with a moderate cell volume dispersion fill the right upper corner of the $w - s$ diagram and there is no upper bound of w, s as it was already mentioned above.

When moving from the PVT point down to the left lower corner, positions of tessellations with wide and gradually more pronounced multimodal cell volume distributions are encountered (generating processes are Bernoulli globular cluster fields with variable implantation probabilities p) and Johnson-Mehl model with the unimodal very wide cell volume distribution. In the relatively narrow wedge-shaped area lying between the curves describing the Johnson-Mehl model and tessellations generated by Neyman-Scott globular cluster fields with very small value of the cluster size δ are also the positions of tessellations generated by Bernoulli globular cluster fields with higher values of δ . The tessellations of all these types are suitable models for grains of various ferritic and austenitic steels after standard thermal treatment. Consequently, the methods of grain size estimation used in technical practice are based on the assumption that the tessellations characterized by the points $\{1.16, 4.84\}$ (U.S. Standards ASTM E112) or $\{1, 4.505\}$ (Czech Standards ČSN 42 0462) are suitable universally valid models (see the discussion in [12], [18], [19]).

The whole area of the $w - s$ diagram lying below the curves of the Johnson-Mehl model and that one describing tessellations produced by Neyman-Scott spherical cluster fields is occupied by tessellations generated by Bernoulli spherical cluster fields with variable implantation probabilities p . They combine large equiaxial cells generated by parent points without implanted cluster with small elongated or flattened cells produced by spherical clusters that are responsible for rather high values of $\mathbf{E}w$, $\mathbf{E}s$ even when the cell volume distribution is strictly bimodal and small cells prevail. Grain size distributions and arrangement of this type can be found in steels after a thermal treatment allowing an exaggerated growth of certain (primary austenitic) grains [18].

When moving away from the central area of displaced cubic tessellations and PVT, the values of the coefficients of variation of cell contents increases: slowly in the direction of the right upper corner (the sectional component prevails) and quickly in the all other directions (mainly due to the cell size dispersion component) – Fig. 5. In particular, all coefficients have a pole in the $\beta = \infty$ point of the Johnson-Mehl model. Along the loops describing tessellations generated by Bernoulli cluster fields, they vary considerably and attain their maxima near the point $p \approx 0.5$ [15].

Finally, it is proposed that the unoccupied part of the $w - s$ plane in the presented figures with arbitrary values of $\mathbf{E}w$ and high values of $\mathbf{E}s$ represents non-convex tessellations with corrugated – perhaps wavy or “fractal-like” – boundaries.

4.4. Applications. The straightforward application of the $w - s$ diagram is the grain size estimation from planar and line section of a 3D space-filling systems. By combining the direct estimates of the intensities λ' , λ'' and of CV v' , the approximate location of the examined grain structure in the $w - s$ diagram can be proposed and the estimates of λ , CV v obtained. The procedure is demonstrated for computer simulated tessellations in [12] and applied to real metallic polycrystals in [18], [19].

REFERENCE

- [1] K. Bodlák, P. Ponížil, I. Saxl: *3D Voronoi tessellation generated by Strauss process*. Proc. 11th Summer school Robust'2000, JČMF, Praha 2001, 1-8.
- [2] M. C. Durand and R. Warren: *Empirical equations for the estimation of number per unit volume of particulate systems*. Stereol. Jugosl. **3** (Suppl. 1) (1981) 109-114.
- [3] H. Hermann, H. Wendrock, D. Stoyan: *Cell-area distributions of planar Voronoi mosaics*. Metallography **23**, (1989), 189-200.

- [4] A. L. Hinde, R. E. Miles: *Monte Carlo estimates of the random polygons of the Voronoi tessellation with respect to a Poisson process*. J. Statist. Comput. simul. **10** (1980), 205-223.
- [5] U. Lorz: *Cell-area distributions of planar sections of spatial Voronoi mosaics*. Materials characterization **3**, (1990), 297-311.
- [6] A. Okabe, B. Boots and K. Sugihara: *Spatial Tessellations*. J. Wiley & Sons, Chichester 1992.
- [7] I. Saxl, I. Kohútek: *Voronoi tessellations generated by Boolean cluster fields*. In: Wojnar L, Roźniatowski K, Kurzydłowski KJ, eds. Proc. Int. Conf. on The Quantitative Description of Materials Microstructure Q-MAT'97. Jagiellonian University, Kraków 1997, 481-488.
- [8] I. Saxl and P. Ponižil: *3D Voronoi tessellations of cluster fields*. Acta Stereol. **17** (1998), 237-246.
- [9] I. Saxl and P. Ponižil: *3D Voronoi tessellations generated by Poisson and lattice cluster fields*. Acta Stereol. **17** (1998), 247-252.
- [10] P. Ponižil and I. Saxl: *Properties of 3D Poisson hard-core and pseudo-hard-core fields II. Voronoi tessellations*. Proc. S⁴G, Int. Conf. on Stereology, Spatial Statistics and Stochastic Geometry, (V. Beneš, J. Janáček and I. Saxl, eds.), JČMF, Praha 1999, 227-239.
- [11] I. Saxl, P. Ponižil: *Spatial Voronoi tessellations generated by non-Poisson point fields*. In: Stochastic Geometry, Stereology and Image Analysis, 24.-28.8.1999. University of Calgary, Calgary 1999, 25-26 and the full length version of the lecture at <http://fyzika.ft.utb.cz/voronoi/>.
- [12] I. Saxl, K. Sülleiová and P. Ponižil: *Simulating grain size estimation*. Kovové materiály **39**, (2001), 396-409.
- [13] I. Saxl, P. Ponižil: *Shape of Voronoi cells*. Proc. 11th Summer school Robust'2000, JČMF, Praha 2001, 284-297.
- [14] I. Saxl, P. Ponižil: *Grain size estimation: $w - s$ diagram*. Materials Characterization **46** (2001), 113-118.
- [15] I. Saxl, P. Ponižil: *Bernoulli cluster fields: Voronoi tessellations*. Appl. Math. **47** (2002), 156-167.
- [16] D. Stoyan, W. S. Kendall and J. Mecke: *Stochastic Geometry and its Applications*. J. Wiley & Sons, New York (1995).
- [17] D. Stoyan, H. Stoyan: *Fractals, Random Shapes and Point Fields*. J. Wiley, Chichester, 1994.
- [18] A. Ševčík, K. Sülleiová, M. Besterci, I. Kohútek and I. Saxl: *Grain size estimation in steels*. Kovové materiály **40**, (2002), 85-98.
- [19] O. Velgosová, I. Saxl, and M. Besterci: *Microstructural characteristics of dispersion strengthened Cu-based system*. In: P. Šandera (ed.): Proc. 3rd Int. Conf. on Materials Structure & Micromechanics of Fracture, University of Technology, Brno 2001, CD ROM, 223-231.

MATHEMATICAL INSTITUTE, ACADEMY OF SCIENCES OF THE CZECH REPUBLIC, ŽITNÁ 25,
CZ 115 67 PRAHA 1

DEPARTMENT OF PHYSICS, TOMAS BATA UNIVERSITY, NÁMĚSTÍ TGM 275, CZ 762 72, ZLÍN